Synthesis of Core–Shell PtRu Dendrimer-Encapsulated Nanoparticles. Relevance as Electrocatalysts for CO Oxidation

DATASET

Synthesis of Core−Shell PtRu Dendrimer-Encapsulated Nanoparticles. Relevance as Electrocatalysts for CO Oxidation†

María Bernechea,‡ Sergio García-Rodríguez,§ Pilar Terreros,§ Ernesto de Jesús,‡ José L. G. Fierro,*,§ and Sergio Rojas*,§

Departamento de Química Inorgánica, Universidad de Alcalá, Campus Universitario, E-28871 Alcalá de Henares, Madrid, Spain, and Grupo de Química y Energía Sostenible, Instituto de Catálisis y Petroleoquímica, CSIC, C/Marie Curie 2, E-28049, Madrid, Spain

Received: July 20, 2010; Revised Manuscript Received: November 10, 2010

The synthesis of PtRu nanoparticles has been accomplished by using the dendrimer-encapsulated nanoparticle (DEN) approach. We report that the surface distribution of the particles can be tuned by suitable control of the reaction pathway. The present study focuses on the synthesis and characterization of Pt and PtRu nanoparticles and the evaluation of their performance as CO_{ad} electro-oxidation catalysts. Bimetallic Pt/Ru particles displaying Ru-core Pt-shell (Ru@Pt) and Pt-core Ru-shell (Pt@Ru) structures, in which Ru or Pt are preferentially located on the outermost layer of the nanoparticles, have been synthesized. Characterization data confirm the formation of the bimetallic particles with the desired atomic distribution. The importance of the actual nature of the bimetallic samples in the CO_{ad} electro-oxidation reaction has been discussed.

1. Introduction

Transition metal nanoparticles (NPs) containing from a few dozen to several thousand atoms have a unique performance in many fields such as catalysis, biological applications, semiconductors, magnetic materials, and so on.[1] Their unique performance is due to their small size, within the nanometer range, narrow size distribution, and the increase in the portion of surface/interface atoms. This is particularly important for the design of catalysts, as decreasing the mean size of the particles renders it possible to increase the dispersion, that is, the percentage of exposed sites, hence increasing their mass activity.[2] Many approaches to the synthesis of nanoparticles have been described.[3−6] The so-called bottom-up approaches involve the reduction of encapsulated ions or salt precursors stabilized by different capping agents such as polymers, surfactants, thiols, or dendrimers, among others.[7,8]

The reproducibility and fine-tuning of nanoparticle composition and/or morphology are serious issues to be resolved. Among the many routes for synthesizing nanoparticles, the dendrimer-encapsulated nanoparticle approach is attractive due to its intrinsic advantages, such as obtaining well-defined particles of uniform size and composition.[9,10] Dendrimer-encapsulated nanoparticles (DENs) are prepared in two steps. First, metal-precursor ions are extracted into dendrimers by coordination with their inner functional groups in fixed stoichiometries. The nature and number of the functional groups can be controlled by choosing the type of dendrimer and its generation. Second, the intradendrimer metal ions are reduced to yield metallic nanoclusters, which remain stabilized within the dendrimer, thus precluding their agglomeration. This process leads to stable, nearly size-monodisperse nanoparticles.[11,12] More importantly, at least when it comes to catalyst synthesis, if a mixture of two metal-precursors ions is added, alloyed bimetallic nanoparticles with different compositions can be obtained. It is also possible to generate core−shell structures using a sequential metal loading, i.e., by adding the second metal ions after the reduction of the first metal.[9,10,13]

Monometallic and bimetallic DENs have previously proven to be active catalysts both in homogeneous and heterogeneous processes.[9,10,14−17] The catalytic performance of Pt and Pt−Pd DENs in the oxygen reduction reaction (ORR) has been studied recently.[18−21] However, studies dealing with the preparation of DEN electrocatalysts for electro-oxidation reactions are scarce. Carbon-supported PtRu[22] and PtSn[23] bimetallic catalysts are the most efficient formulations for the electro-oxidation of CO and methanol, especially the former ones. This is because Ru or Sn, being more oxophilic than Pt, are able to generate $-OH_{ad}$ species at less positive potentials than Pt. Such $-OH_{ad}$ species are necessary during the electro-oxidation of CO or methanol.[23] It is also well-known that the actual morphology of the catalysts has a marked influence on the actual performance of Pt catalysts.[24] Numerous methods have been proposed for the synthesis of PtRu nanoparticles.[25] It is only very recently that the synthesis of PtRu DENs for methanol electrooxidation has been reported.[26]

In principle, the catalytic performance of a material will be governed by the composition and morphology of its outermost layer. Nonetheless, the influence of subsurface atoms can prevail in processes such as the oxygen reduction reaction[27] or the preferential oxidation of carbon monoxide in hydrogen.[28,29] In this sense, the actual distribution of atoms in a catalyst, rather than its composition, is the parameter that informs catalytic performance. In consequence, describing synthetic routes that allow synthesizing materials with high specific metal surface area of controlled composition, size, and morphology is of great interest. The correlation between the design of Pt-based nanoparticles and their performance for fuel cell applications has been revised recently.[30]

The present study reports the synthesis of bimetallic core−shell Pt−Ru DENs prepared by following a sequential metal loading. Remarkably, this synthetic approach is flexible enough to permit

† Part of the "Alfons Baiker Festschrift".

* To whom correspondence should be addressed. E-mail: srojas@icp.csic.es; jlgf@icp.csic.es.

‡ Departamento de Química Inorgánica, Universidad de Alcalá.

§ Instituto de Catálisis y Petroleoquímica, CSIC.

10.1021/jp106728s
Published on Web 12/21/2010

a proper control of the actual location of the Pt and Ru atoms on the bimetallic nanoparticles by adjusting the appropriate parameters during the synthetic path. Thus, materials of similar atomic composition and size, albeit displaying different core−shell structures, either as Ru@Pt or Pt@Ru, have been synthesized. Furthermore, to the best of our knowledge, this is the first time the dendrimer approach has been successfully used for the synthesis of core−shell Pt−Ru nanosized particles.

The performance of the PtRu particles as catalysts for the CO_{ad} electro-oxidation has been studied, and the influence of their actual structure and atomic distribution is correlated with their catalytic properties.

2. Experimental Methods

Chemicals and Materials. All reactions were performed using standard Schlenk techniques under an argon atmosphere. The fourth-generation hydroxyl-terminated PAMAM dendrimer (PAMAM G4-OH) with an ethylenediamine core was obtained as 17.72% methanol solutions from Dendritech, Inc. Prior to use, the methanol was removed under vacuum. K_2PtCl_4 and $RuCl_3 \cdot xH_2O$ were purchased from Pressure Chemical Co. and Johnson Matthey, respectively; cellulose dialysis sacks (cutoff of 12400 Da), $NaBH_4$, $HClO_4$ (70%), and Nafion (5%) were purchased from Aldrich; and Carbon Vulcan XC-72R was purchased from CABOT. All these reagents were used as received without further purification. Milli-Q water (type II quality; obtained with a Millipore Elix 10 UV Water Purification System) was used to prepare all the aqueous solutions.

2.1. Preparation of Pt DENs. The Pt DENs were prepared according to the previously reported method.[20,21] Briefly, 62.5 μL of the methanolic solution of PAMAM G4-OH was evaporated to dryness and subsequently diluted with 18 mL of Milli-Q water. An amount of 250 μL of 0.1 M aqueous solution of K_2PtCl_4 was added, and this mixture was stirred for 3 days. This results in the theoretical encapsulation of an average of 40 Pt^{2+} ions within each dendrimer. The dropwise addition of a 10-fold molar excess of $NaBH_4$ (9.4 mg in 2 mL of water) reduced the ions to Pt^0. After one day of stirring, the resulting solution was dialyzed against water for 24 h to remove the remaining ions. Finally, the volume of the solution was fixed at 25 mL and stored in darkness.

2.2. Preparation of Core−Shell Ru@Pt and Pt@Ru DENs. The residue obtained after evaporating the solvent from 62.5 μL of a methanolic solution of PAMAM G4-OH was dissolved in 18 mL of Milli-Q water. An amount of 125 μL of 0.1 M aqueous solution of K_2PtCl_4 (Pt@Ru), or $RuCl_3 \cdot xH_2O$ (Ru@Pt), was added to this aqueous solution, and this mixture was stirred for 3 days. This results in the theoretical encapsulation of an average of 20 ions (Pt^{2+} or Ru^{3+}) within each dendrimer. The dropwise addition of a 10-fold molar excess of $NaBH_4$ (4.7 mg in 1 mL of water) reduced the ions to Pt^0 or Ru^0. After one day of stirring, the resulting solution was dialyzed for 24 h against water to remove the remaining ions ensuring thus a neutral pH before the addition of the second metal precursor. An amount of 125 μL of 0.1 M aqueous solution of $RuCl_3 \cdot xH_2O$ (Pt@Ru), or K_2PtCl_4 (Ru@Pt), was added to this solution, and this mixture was stirred for 3 days, treated with a 10-fold molar excess of $NaBH_4$ (4.7 mg in 1 mL of water) for 24 h, and dialyzed against water for 24 h to remove the remaining ions. Finally, the volume of the solution was fixed at 25 mL and stored in darkness. Precipitate is observed in the Ru@Pt solutions.

2.3. Characterization. UV−vis absorbance spectra were recorded using quartz cells on a Perkin-Elmer Lambda 18 UV−vis spectrometer. For the ICP−MS analysis, the aqueous samples were diluted with 1% HNO_3 and then analyzed with an ELAN-6000 ICP-MS unit (Perkin-Elmer Sciex, Ontario, Canada) under the following instrumental conditions: RF power of 1200 W, nebulizer gas flow of 0.8 L/min, lens setting as auto lens, cross-flow nebulizer, and nickel cones. The ICP−MS acquisition settings were as follows: dwell time of 50 ms, number of sweeps equal to 30, 5 replicates, peak hopping scan mode, 1 MCA channel per peak, and a dual detector mode. All the samples were analyzed under the same instrumental conditions. Transmission Electron Microscopy (TEM), High-Resolution Transmission Electron Microscopy (HRTEM), and High-Angle Annular Dark Field (HAADF) images were obtained using a TEM JEOL 2100F microscope operating with an accelerating voltage of 200 kV. Samples were prepared by placing two drops of the aqueous solutions on a holey-carbon-coated grid and allowing the solvent to evaporate in air. The average diameter was calculated by measuring the diameters of no less than 100 randomly selected metal particles from the nonaggregated areas in at least two micrographs of each sample. An INCAx-sight (Oxford Instruments Ltd.) Energy Dispersive X-ray Spectrometer (EDS) was used, and the spectra were analyzed with the INCA-EnergyTEM Suite v4.06 software. Pt−*L* and Ru−*L* energy lines were used for quantification, according to a Cliff-Lorimer routine with theoretical *k* factors included in the software. The contrast in the HAADF images is mainly due to Rutherford scattering, which is a function of *Z*. The more intense regions correspond to the Pt−Ru particles that are supported on the amorphous carbon film of the TEM grid. The beam was scanned across one nanoparticle, and EDS was acquired simultaneously. Experimental conditions were as follows: dwell time of 100 ms, and line profiles were performed with a scan resolution of 128 points along scanned length and a beam size of 0.7 nm. The software stores the collected spectra and the position of the beam in a data cube for further statistical analysis. X-ray photoelectron spectra (XPS) of the samples were acquired with a VG Escalab 200R spectrometer fitted with an Mg Kα ($h\nu$ = 1253.6 eV) 120 W X-ray source. The energy regions of the photoelectrons of interest were scanned until a good signal-to-noise ratio was achieved. Intensities were estimated by calculating the integral of each peak, determined by subtracting the Shirley-type background and fitting the experimental curve to a combination of Lorentzian and Gaussian lines of variable proportions. Accurate binding energies ($\pm$0.2 eV) were determined by referencing to the C 1s peak at 284.6 eV. Diffuse Reflectance Infrared Fourier Transform (DRIFT) spectra were acquired in a Jasco 4100 spectrometer using a praying mantis cell. The samples were prepared by stirring 2 mL of the corresponding aqueous DEN solution overnight with 500 mg of α-Al_2O_3 and then drying the mixture at 100 °C, also overnight. The background was recorded in KBr. 128 scans were measured for each spectrum. The treatment of the samples was in He for 5 min at 100 °C, then H_2 at 130 °C for 15 min to reduce the sample, and then CO at rt for 15 min, and finally, He was flowed at rt for 10 min. For the electrochemical experiments, the samples were deposited onto the working electrode as an ink. Inks were prepared by sonicating a mixture of 2 mg of Vulcan XC-72R carbon, 10 μL of Nafion, and 1 mL of the corresponding DEN solution. An amount of 10 μL of the corresponding ink was deposited onto the working electrode (glassy carbon electrode, 3 mm diameter), and the solvent was then allowed to evaporate in air at room temperature. Prior to each test, the electrode was polished with 0.05 μm alumina to obtain a mirror finish and rinsed with triply distilled water in

an ultrasonic bath. All experiments were performed at room temperature in a conventional three-compartment electrochemical glass cell. A graphite cylinder and an Ag/AgCl electrode were used as the counter and reference electrodes, respectively. In this manuscript, potentials are reported versus the normal hydrogen electrode (NHE). During the measurements, a gentle flow of nitrogen was maintained over the electrolyte surface. Measurements were taken with a computer-controlled EG&G 273A potentiostat/galvanostat. Before the CO_{ad} stripping studies, the electrodes were activated by scanning the potential between 0 and 0.8 V (for Pt−Ru DENs) and 1 V (for Pt DENs). At least 10 cycles at 50 mV/s and 5 cycles at 10 mV/s were measured until reproducible cyclic voltammograms were obtained. For the CO_{ad} stripping measurements, CO was flowed, while the electrode was set at a constant potential of 20 mV for 15 min. Ar was then bubbled for a minimum of 30 min to purge the CO out of the solution. Finally, three consecutive cycles between 0 and 1 V at 10 mV/s were recorded.

3. Results and Discussion

3.1. Synthesis and Characterization of PtRu Nanoparticles. The dendrimer templating method[20,21] has been used to prepare Pt−Ru nanoparticles (1:1 molar ratio) presenting two different structures, namely, Pt-core/Ru-shell and Ru-core/Pt-shell (denoted henceforth as Pt@Ru and Ru@Pt, respectively). Pt DENs (denoted Pt) have been synthesized and used as reference material. The metal-to-dendrimer molar ratio of 40:1 has been chosen. According to the literature,[31,32] a minimum of three days is necessary for a complete encapsulation of Pt^{2+} and Ru^{3+} ions within the dendrimers, prior to the reduction to give the nanoparticles. In fact, color changes are detected in all the steps of nanoparticle synthesis, and the evolution of the reactions can be followed by UV−vis spectroscopy (see Figures S1−S3 in Supporting Information). Figure 1a depicts the UV−vis spectra of the Pt@Ru and Ru@Pt, together with the spectra of Pt and Ru DENs (Ru) for comparative purposes. The spectra display distinct features in line with the different structure of each sample. The spectrum of the monometallic Pt DENs is similar to others already reported,[20,21] showing a monotonically increasing band and small peaks at ∼225 and ∼250 nm, while that of Ru DENs presents a small peak at ∼212 nm and a characteristic shoulder at ∼280 nm.[31,32] The spectrum of Pt@Ru shows two peaks at ∼217 and ∼245 nm, indicating that the electronic transitions are different from those of the monometallic samples. The adsorption at ∼280 nm has been ascribed to Ru−amine complexes.[26,32] Some authors have proposed that such species cannot be stabilized at acidic pH because of the protonation of the amine and amide groups of the dendrimer.[26,32] The observation of the band at ∼280 nm (Figure S2, Supporting Information) implies that the pH value of solution before Ru addition is not acid. Moreover, a simulated spectrum resulting from the combination of Pt and Ru spectra is depicted in Figure 1b. This spectrum presents two absorbances at ∼217 and ∼255 nm. The difference in energy of the higher-wavelength absorption (255 nm) compared with that of the bimetallic samples (245 nm) is 1600 cm^{-1}. This difference is high enough to deduce a platinum−ruthenium interaction.

With regard to the Ru@Pt sample, a broad peak centered at ∼245 nm is observed, with a fall below zero of the absorbance at short wavelengths. This latter finding could be due to the precipitation of some metal and dendrimer, generating a black solid in suspension, which is always observed in these solutions. It should be noted that particle agglomeration has previously been observed in other platinum-shelled systems, especially

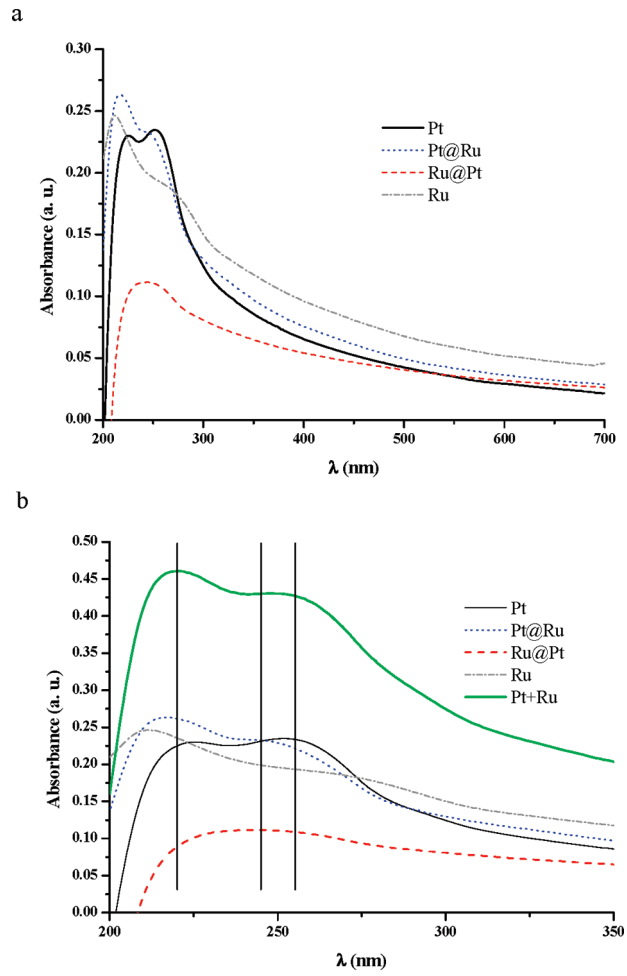

Figure 1. (a) UV−vis spectra of Pt, Pt@Ru, Ru@Pt, and Ru DEN aqueous solutions measured taking dendrimer aqueous solutions as blank. The metal concentration in each case is 5×10^{-5} M. (b) Magnification of the UV−vis spectra between the 200 and 350 nm zone. The spectrum resulting from combining Pt and Ru spectra is also included.

TABLE 1: Metal Concentration (mg/L) in the DEN Aqueous Solutions Determined by ICP−MS

	nominal values		experimental values	
	Pt	Ru	Pt	Ru
Pt	195.078	-	137.744	-
Pt@Ru	97.539	50.535	46.852	35.776
Ru@Pt			41.208	12.134

when the Pt shell is thin.[29] In fact, the ICP−MS analyses of the aqueous samples show that some metal is lost during the synthetic process, especially in Ru@Pt (see Table 1). Indeed, metal losses have already been described for similar platinum systems, and the presence of a certain amount (∼20%) of nondendrimer-coordinated platinum ions has also been measured.[15,31,33] In spite of metal leaching, the molar ratio extracted from these analyses coincides well with the nominal metal ratio Pt:Ru 1:1, except for the Ru@Pt sample. Moreover, the stability of the DENs in aqueous solutions has also been measured. The UV−vis spectra of the samples recorded after 10 weeks of storage under nitrogen atmosphere reveal that samples are stable (spectra depicted in Figure S4, Supporting Information).

The oxidation state of Pt and Ru species was analyzed by XPS. The atomic surface abundance and binding energies recorded for the Pt $4f_{7/2}$ and Ru $3p_{3/2}$ core-level regions of the samples are shown in Table 2. The spectra of the Pt region of

TABLE 2: Binding Energies (eV) and Surface Atomic Ratios of DEN Samples[a]

sample	Pt $4f_{7/2}$	Ru $3p_{3/2}$
Pt	71.0 (27)	-
	72.4 (48)	
	74.3 (25)	
Pt, H_2-treated	71.0 (44)	-
	73.0 (50)	
	74.9 (6)	
Pt@Ru	71.6 (20)	
	72.8 (49)	462.2 (56)
	74.9 (31)	464.1 (44)
Pt@Ru, H_2-treated	71.3 (20)	
	73.4 (55)	461.4 (70)
	74.5 (25)	463.5 (30)
Ru@Pt	72.0 (47)	
	73.6 (34)	461.7 (45)
	75.0 (19)	463.8 (55)
Ru@Pt, H_2-treated	71.2 (36)	
	73.3 (45)	460.6 (74)
	74.7 (19)	462.3 (26)

[a] Binding energies (eV) are referred to the C 1s peak at 284.6 eV. H_2 treatment: 1 h at 150 °C in H_2 flow.

all samples are composed of three doublets whose maxima appear at ca. 71.0 eV ascribed to Pt^0, 72.5 eV ascribed to Pt^{2+}, and 74.5 eV to Pt^{4+} species.[34] It is not unlikely that reduced and oxidized Pt and Ru species coexist within nanosized particles.[35] This can be explained by the interaction of Pt with dendrimer residues or simply by air exposure that will result in partial oxidation of the outermost layers of the particles. Upon hydrogen treatment at 150 °C, Pt^0 becomes the predominant one, especially at the expense of the more oxidized forms of Pt. Noticeably, the relative amount of Pt^0 in Pt@Ru is the lowest in the series, and so it remains even after the reduction treatment. In the same line, Ru^0 species, identified by a peak centered at binding energies around 280 eV, become predominant in all samples after the thermal treatment in hydrogen. The position of the Pt $4f_{7/2}$ peaks of the bimetallic samples is shifted to higher binding energies relative to the monometallic sample. This result is in line with published data, suggesting an interaction between Pt and Ru.[28]

A useful way of analyzing the surface composition of metallic particles consists of adsorbing probe molecules such as CO and recording variations in their vibrational energy upon adsorption. It has previously been reported that the vibrational stretching mode of linearly adsorbed CO (υ_{COL}) appears in the 2080−2060 cm^{-1} region for Pt and in the 2025−1995 cm^{-1} region for Ru nanoparticles. Pt/Ru alloyed particles record a CO_{ad} peak in the intermediate region (2060−2025 cm^{-1}).[36] DRIFT (Diffuse Reflectance Infrared Fourier Transform) spectra of the DEN samples are shown in Figure 2. The DRIFT spectrum of Pt DENs presents a CO_{ad} peak at 2060 cm^{-1}. The Pt@Ru DENs record a single CO_{ad} peak at 1994 cm^{-1}, which has been ascribed to linearly adsorbed CO species on Ru^0 with a high amount of defect sites and/or isolated Ru^0 sites surrounded by partially oxidized $Ru^{\delta+}$ sites.[37] It is well admitted that the density of edge-corner sites increases with the decreasing size of the particles, hence resulting in a redshift of the υ_{COL}.[38,39] This result confirms that the outermost layer of Pt@Ru contains predominantly ruthenium. The CO_{ad} peak on Ru@Pt DENs appears at 2027 cm^{-1}. This position is in line with a higher Pt/Ru ratio on the surface of Ru@Pt as compared to Pt@Ru. The observation of a single peak between the Pt−CO_{ad} and Ru−CO_{ad} peaks suggests that bimetallic PtRu particles are obtained. The peaks appearing between 1890 and 1780 cm^{-1} are ascribed to the

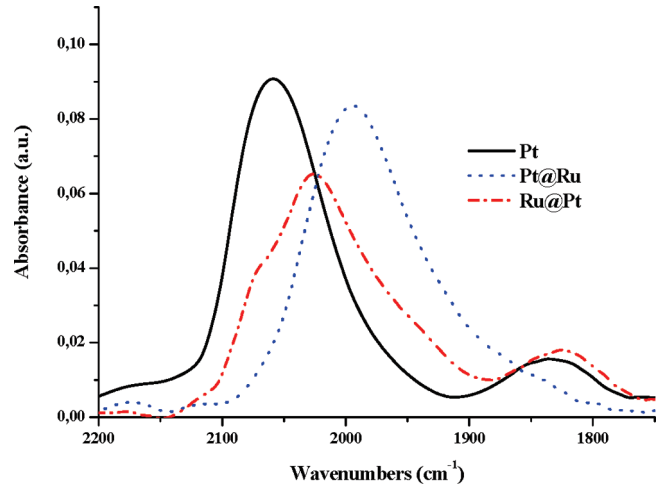

Figure 2. DRIFT spectra of Pt, Pt@Ru, and Ru@Pt DEN aqueous solutions deposited onto γ-Al_2O_3.

stretching mode of bridge-type CO on Pt.[36] All samples record a broad peak in this region except Pt@Ru as expected for Ru-enriched surfaces.

From the DRIFT results, and in good agreement with UV−vis ones, it can be concluded that a Pt−Ru electronic interaction takes place in the bimetallic samples, irrespective of their atomic distribution. More importantly, DRIFT results pinpoint their different morphologies. Thus, the surface of Pt@Ru is enriched in Ru, while Pt is the predominant element on the surface of Ru@Pt. Although the surface of the core−shelled particles is enriched with one of the metals, Ru in sample Pt@Ru or Pt in sample Ru@Pt, it is not unlikely that the actual composition of the surface contains both elements. Considering this line of reasoning, the results described above fit well.

Yet another factor should be taken into account to explain our results concerning atom distribution. Surface enrichment of Ru after heating in H_2 has been reported for PtRu samples.[40] For the bimetallic particles reported here, a slight enrichment in Ru is deduced from the DRIFT spectra for all samples, probably as a result of the thermal treatment in hydrogen prior to CO admittance (see Experimental Section for further details). Remarkably, a Pt−Ru interaction is found in all bimetallic samples, with no evidence of isolated Pt- or Ru-clusters being observed.

The transmission electron microscopy images depicted in Figure S5 (Supporting Information) show monodisperse and roughly spherical nanoparticles with a mean particle size of 1.6 ± 0.6 nm for Pt DENs, 1.6 ± 0.7 nm for Pt@Ru, and 2.4 ± 0.6 nm for Ru@Pt. XRD analysis (see Figure S6, Supporting Information) records no reflections of any Pt_{fcc} crystal phases, confirming that the grain size is <2 nm. The size of the Pt DENs is larger than the theoretical value of 1.1 nm calculated for the clusters expected from the metal-to-dendrimer molar ratio used in this manuscript[10,41] but identical to other reported experimental values.[10,21,41,42] A number of reasons have been suggested for this discrepancy: (i) the theoretical value has been calculated by assuming a spherical shape, and the real shape of these nanoparticles can be slightly different (for instance, nonclose-packed geometries) or (ii) the smaller nanoparticles are not detected, and the observed mean size is biased to larger values.[9,10,17] Particles are randomly oriented on the TEM grid and have different shapes. Figure 3a is an HRTEM micrograph of the Pt DENs sample showing a maximum diameter of ca. 2 nm. The figure in the left is the indexed digital diffraction pattern

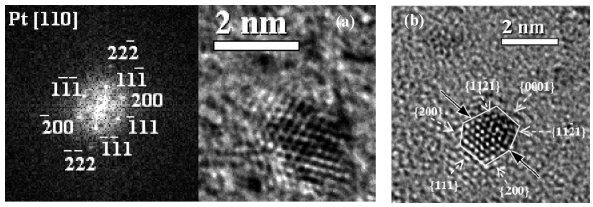

Figure 3. HRTEM images of (a) Pt and (b) Pt@Ru. The left image in figure (a) is an electron diffraction diagram of the particle in the right side of the figure. Black arrows in figure (b) show a twinning plane.

of the particle, obtained after calculation of the Fast Fourier Transform of the image. The stacking order of the $(11\bar{1})$ planes follows the sequence ABCABC in line with the fcc structure expected for Pt. Figure 3b is an HRTEM image of the Pt@Ru sample showing a particle of about 1.8 nm exhibiting a twinning plane. The (111) planes are stacked parallel to the arrows. The planes on the left of the arrow exhibit an fcc structure, with a stacking order ABC; however, the (0001) planes at the right of the arrow are stacked following the order ABA, typical of the hcp structure. Twinning is scarcely observed in Pt particles[43] but frequently observed in Pt−Ru samples.[44]

Figure 4 shows EDS profiles of the $PtM_{\alpha 1}$ and $RuL_{\alpha 1}$ energy lines of the Pt@Ru (Figure 4a) and Ru@Pt (Figure 4b) samples. These profiles reveal, and confirm, the predominance of the desired atom (Ru or Pt, respectively) on the surface of the particle. This result confirms that the dendrimer strategy allows the synthesis of core−shell structures. Furthermore, the synthetic strategy described in this manuscript allows the selective location of the desired metal either as the core or as the shell layer.

At this point, a more detailed discussion is required on the morphology expected for the bimetallic particles. Nanoparticles with a complete and regular outer geometry, such as a cuboctahedron habit in our case (see TEM results), are designated as full-shell or "magic number" clusters. The number of atoms in those structures is given by eq 1.

$$y = 10n^2 + 2 \quad (n > 0) \tag{1}$$

where y is the total number of atoms in a layer and n is the number of shells around a single metal atom.[45] Consistent with previous reports,[9,10,21,41,42] the metal to dendrimer molar ratio used in this manuscript would lead to the formation of 40 atom-

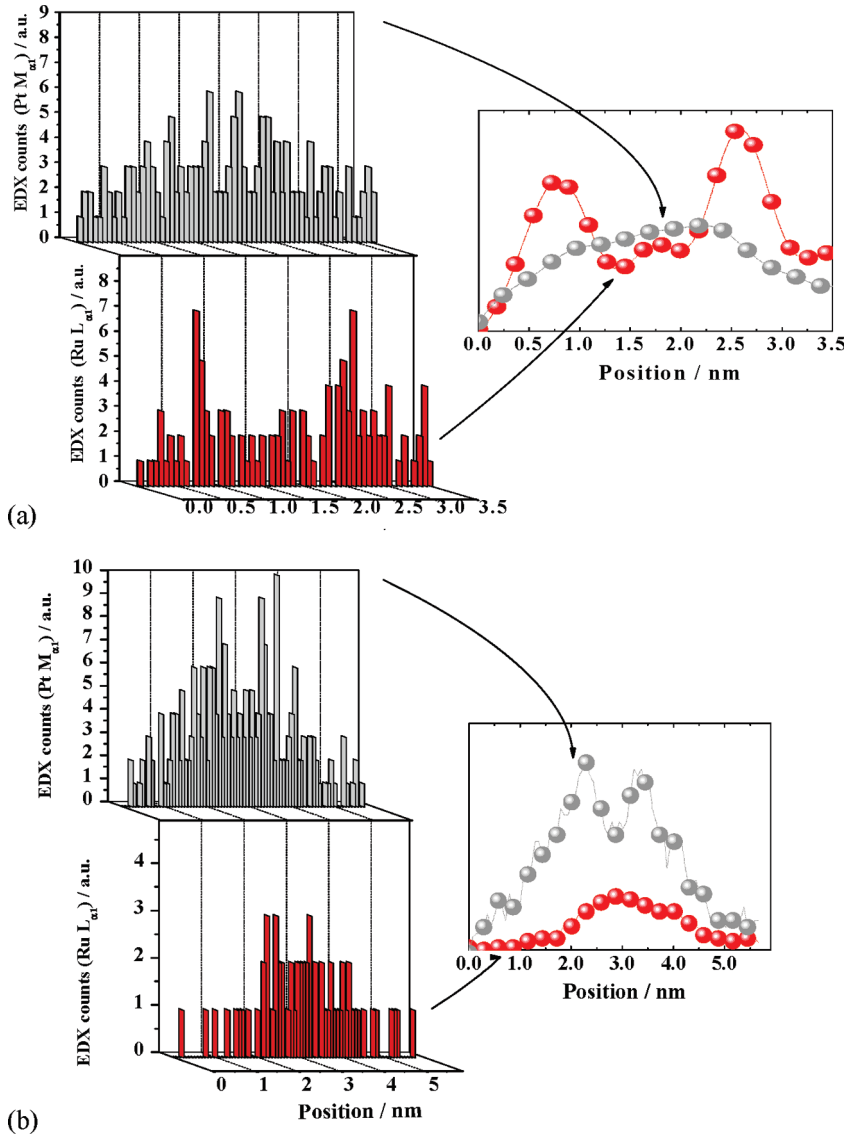

Figure 4. EDS profiles of the $PtM_{\alpha 1}$ and $RuL_{\alpha 1}$ energy lines and smoothed curves of the profiles measured from a Pt@Ru particle (a) and from a Ru@Pt particle (b) clearly showing the core−shell structure of the particle with a preferential distribution of Ru (a) or Pt (b) in the outer part of the particle.

averaged particles. To fulfill eq 1, particles of sizes like those found in this manuscript should contain at least 55 atoms, with 40 of them located on their outer shell. Consequently, to satisfy the atomic stoichiometry imposed by our synthesis, both Pt and Ru atoms should coexist in the outermost layer. This line of reasoning is supported by our experimental results, revealing the coexistence of both Pt and Ru on the surface of the bimetallic particles; however, the surface predominance of each atom can be controlled by adjusting the synthetic parameters as suggested by experimental results and further endorsed by the EDS profiles depicted in Figure 4.

In summary, we have synthesized PtRu core−shell DENs using the sequential metal loading approach, which has only previously been used for the synthesis of PdAu and AuAg DENs.[13] On the other hand, although the synthesis of Ru-core/Pt-shell particles using a sequential polyol process has recently been reported,[28] the synthetic approach reported here permits a more precise control of the morphology of the particles, thus allowing the synthesis of Pt-core/Ru-shell particles and the preparation of mono- and bimetallic samples with very similar sizes.[26]

3.2. Immobilization of DENs on Glassy Carbon Electrodes. To evaluate the catalytic performance of the different samples as CO electro-oxidation catalysts, DENs were deposited onto Glassy Carbon Electrodes. First, taking into account the results published in the literature,[19−21] a direct immobilization of DENs on glassy carbon electrodes was attempted. However, the electrochemical response thus obtained was very weak and finally declined after a few cycles. Finally, immobilization was successfully achieved by depositing an ink onto the electrode and allowing the solvent to evaporate in air at room temperature (see Experimental Section). This methodology provides several advantages, with one being that the catalysts remain attached to the surface of the electrode maintaining electric communication throughout all the experiments, and the amount of catalyst deposited is known exactly. Moreover, catalyst deposition following this procedure results in higher current densities for Pt DENs than for identical or bigger Pt-DENs reported in the literature (see below).[19−21]

3.3. Electrochemical Measurements. The cyclic voltammograms of the Pt and PtRu DEN samples are shown in Figure S7 (Supporting Information). The potential region between $0 < E < 0.4$ V is known as the hydrogen region or H_{upd} region, and it records the peaks for the formation of absorbed H (negative current) and the oxidation of adsorbed H (positive current).[46] The intensity and shape of the peaks is characteristic of the electrode appearing well-defined in pure Pt electrodes. As can be seen, the hydrogen adsorption−desorption features of the Pt@Ru DENs are very weak, as if a core−shell structure had been achieved, and there were no platinum atoms on the surface able to interact with hydrogen. For the other catalysts, the intensity of the H_{upd} region follows the order Pt DENs > Ru@Pt, in agreement with the actual platinum loading of each sample (see Table 1).

The voltammograms corresponding to the CO_{ad} oxidation (CO_{ad} stripping) on the different samples are depicted in Figure 5. Voltammograms recorded before CO admission and after the CO_{ad} oxidation cycle are also depicted. It is observed that the voltammogram corresponding to CO_{ad} oxidation lacks H_{upd} features in the forward scan, which are clearly observed in the other voltammograms. The H_{upd} ability is fully recovered once CO_{ad} has been fully oxidized. In fact, the voltammogram recorded after the CO_{ad} stripping cycle shows H_{upd} features identical to those recorded before CO admission. CO_{ad} oxidation

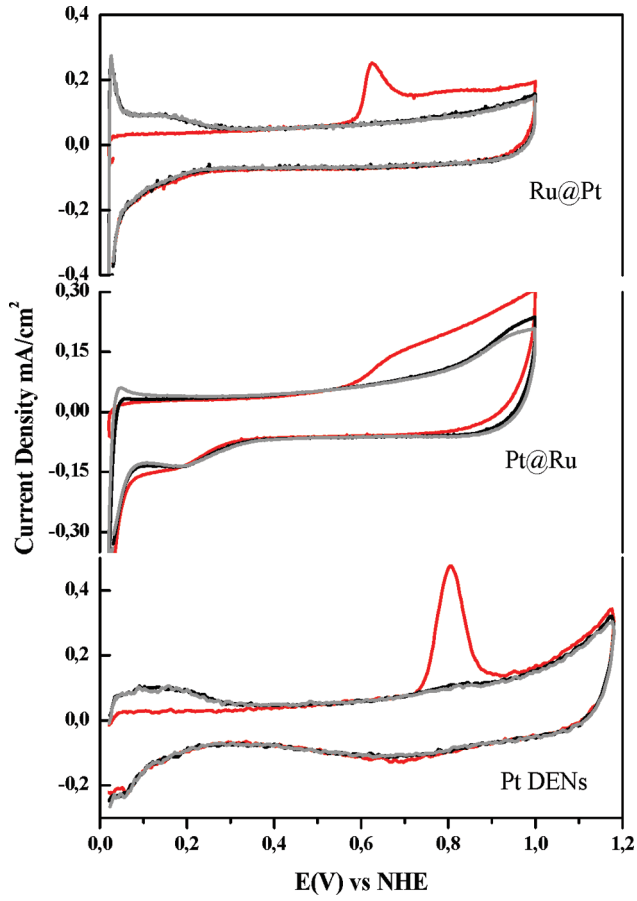

Figure 5. CO_{ad} stripping (red line) experiments obtained for Pt, Pt@Ru, and Ru@Pt DENs. The voltammograms in gray and black were recorded immediately before CO admission and after the CO_{ad} stripping cycles. Electrolyte solution = 0.5 M $HClO_4$. Scan rate = 10 mV/s.

TABLE 3: Summary of the Electrochemical Parameters Extracted from the CO_{ad} Stripping Analyses of the Bimetallic Samples and Selected Values Reported for Similar Samples

sample	E_{peak} (V)	charge (μC)$_{CO}$	charge (μC)$_{H\text{-}des}$	EAA[a] (m^2/g_{Pt})	EAA % loss	ref
Pt	0.81	218	123	43[b]	-	this work
Pt@Ru	0.70	150	51	133[c]	57	this work
Ru@Pt	0.62	224	94	129[c]	2	this work
Pt_{55}	0.9−0.93	14	3.2		-	20
Pt_{240}	0.9−0.93	360	126		-	20
Pt_{180}			29.4−46.2	160−222[d]	-	19

[a] Electrode active area (EAA) calculated from the CO_{ad} stripping analysis assuming 420 μC cm^{-2} for CO and 210 μC cm^{-2} for H-des. [b] Calculated from the H-des area. [c] Calculated from CO stripping area. [d] Calculated from H-des area. Pt grams theoretically calculated.

on Pt DENs commences at 680 mV, displaying the Ep_{CO} at 810 mV. These values are shifted to more positive potentials than those reported for state-of-the-art carbon-supported Pt catalysts but in line with the values recorded for small (1−2 nm) Pt particles.[39,47] However, it is interesting to remark that CO_{ad} electro-oxidation on our Pt DENs takes place at lower potentials than on other Pt particles prepared by the same methodology, which have similar or even bigger sizes[20] (see Table 3).

As expected, the presence of ruthenium causes a shift of the CO_{ad} oxidation peak of ∼200 mV to less positive potentials. This feature is well documented, being ascribed to either or both the ligand mechanism (modification of the electronic

properties of the active site decreasing the Pt−CO bond strength) or/and the bifunctional effect (to the shifting of the potential of OH_{ad} formation).[48] The stripping profile of Ru@Pt displays a single CO_{ad} oxidation peak at ca. 620 mV, and the onset for CO_{ad} oxidation is at ∼560 mV. It can be observed that the H_{upd} region is fully recovered after CO oxidation. The CO_{ad} is oxidized on Pt@Ru over a broad potential region starting at ca. 550 mV. Such broadening of the CO_{ad} oxidation wave with the increasing amount of surface Ru has been observed by Jusys et al.,[49] and it could be indicative of the presence of domains of different composition, the ones at lower potentials corresponding to Ru-enriched zones and those at higher potentials ascribed to Ru-lean areas. From the CO_{ad} oxidation features at high potential, it could be inferred that the amount of surface Pt or isolated Pt clusters is rather high in Pt@Ru. However, a careful inspection of the surface of the Pt@Ru particles reveals the preferential exposure of the {0001} planes of Ru_{hcp} (see Figure 3b). There is ample evidence that Ru {0001} is not very active for the oxidation of CO,[50] hence it is not unlikely that the behavior of Pt@Ru for the CO_{ad} stripping reaction is dominated by the more active Pt atoms rather than by the Ru ones, despite the surface predominance of the latter. In this line, the H_{upd} region in the voltammograms of Pt@Ru is ill defined, in good agreement with predominance of Ru atoms on the surface of the sample.[51]

The electrocatalytic active area (specific surface area/mass of Pt) of the electrodes was evaluated from the H_{upd} region and CO_{ad} stripping analyses; the results obtained along with selected values reported for similar samples are summarized in Table 3. The areas obtained for the catalysts range between 40 and 150 m^2/g_{Pt} and are in good agreement with others reported for Pt[52] or even exceed the area of other PtRu particles.[53]

The stability of the bimetallic samples was studied by recording 50 successive scans between 0 and 1 V. When subjected to potential excursions to 1 V, the $j-E$ response of Pt@Ru is clearly modified. The features of the H_{upd} region become magnified, probably as a result of Ru losses during potential excursion >0.8 V, which in turn lead to Pt enrichment on the surface of the particles. On the other hand, the Ru@Pt catalyst shows higher stability, without significant changes in the CO_{ad} oxidation peak or in the H_{upd} features with the different cycles. In fact, the variation of the EAA of Ru@Pt is only ca. 2%. These observations are in line with the formation of a core−shell structure where the platinum shell hinders the passage and subsequent loss of ruthenium to the electrolyte solution.

4. Conclusions

We report here for the first time the synthesis of core−shell Pt−Ru nanoparticles following the dendrimer templating method, showing that this strategy provides reproducible results in terms of size, composition, and atomic distribution. By this new strategy, it is possible to place the desired metal preferentially either on the surface or in the core of the particles by adjusting the nanoparticle synthesis path. As demonstrated by the electrochemical experiments, the DEN approach results in materials with higher specific surface area than that reported for bimetallic PtRu samples of similar composition. As expected, the presence of ruthenium improves the catalytic performance in the CO_{ad} electro-oxidation reaction in relation to platinum-only species. The best results are obtained for the sample with a platinum-enriched surface, whereby it combines the advantages resulting from the presence of ruthenium with a better stability due to its preferential location in the core of the nanoparticle.

Acknowledgment. We gratefully acknowledge financial support from the Spanish Ministry of Science and Education (project CTQ2008-02918/BQU) and the Community of Madrid (project S-0505/PPQ/0328-03 and Postdoctoral Contract to M. B.). S. G. acknowledges the I3P Program for a fellowship, and S. Rojas acknowledges the CSIC project 200780I017 for its support.

Supporting Information Available: UV−vis spectra following the evolution of the reactions. UV−vis spectra of the samples after 10 weeks of storage under nitrogen atmosphere. TEM images and size distribution histograms of the samples. X-ray diffractogram of Pt-DENs. Cyclic voltammograms and magnification of the hydrogen adsorption/desorption zone of the samples. This material is available free of charge via the Internet at http://pubs.acs.org.

References and Notes

(1) Ozin, G. A.; Cademartiri, L. *Small* **2009**, *5*, 1240.
(2) Bond, G. C. *Surf. Sci.* **1985**, *156*, 966.
(3) Bönnemann, H.; Richards, R. M. *Eur. J. Inorg. Chem.* **2001**, 2455.
(4) Eriksson, S.; Nylén, U.; Rojas, S.; Boutonnet, M. *Appl. Catal., A* **2004**, *265*, 207.
(5) Plieni, M. P. *J. Phys. Chem. C* **2007**, *111*, 9019.
(6) Chaudret, B. *C. R. Phys.* **2005**, *6*, 117.
(7) Ott, L. S.; Finke, R. G. *Coord. Chem. Rev.* **2007**, *251*, 1075.
(8) Astruc, D.; Feng, L.; Ruiz Aranzaes, J. *Angew. Chem., Int. Ed.* **2005**, *44*, 7852.
(9) Scott, R. W. J.; Wilson, O. M.; Crooks, R. M. *J. Phys. Chem. B* **2005**, *109*, 692, and references therein.
(10) Crooks, R. M.; Zhao, M.; Sun, L.; Chechik, V.; Yeung, L. K. *Acc. Chem. Res.* **2001**, *34*, 181, and references therein.
(11) Zhao, M.; Sun, L.; Crooks, R. M. *J. Am. Chem. Soc.* **1998**, *120*, 4877.
(12) Balogh, L.; Tomalia, D. A. *J. Am. Chem. Soc.* **1998**, *120*, 7355.
(13) Peng, X.; Pan, Q.; Rempel, G. L. *Chem. Soc. Rev.* **2008**, *37*, 1619.
(14) Bernechea, M.; de Jesús, E.; López-Mardomingo, C.; Terreros, P. *Inorg. Chem.* **2009**, *48*, 4491.
(15) Hoover, N. N.; Auten, B. J.; Chandler, B. D. *J. Phys. Chem. B* **2006**, *110*, 8606.
(16) García-Martinez, J. C.; Lezutekong, R.; Crooks, R. M. *J. Am. Chem. Soc.* **2005**, *127*, 5097.
(17) Lang, H.; May, R. A.; Iversen, B. L.; Chandler, B. D. *J. Am. Chem. Soc.* **2003**, *125*, 14832.
(18) Ledesma-García, J.; Escalante García, I. L.; Rodríguez, F. J.; Chapman, T. W.; Godínez, L. A. *J. Appl. Electrochem.* **2008**, *38*, 515.
(19) Ye, H.; Crooks, R. M. *J. Am. Chem. Soc.* **2007**, *129*, 3627.
(20) Ye, H.; Crooks, J. A.; Crooks, R. M. *Langmuir* **2007**, *23*, 11901.
(21) Ye, H.; Crooks, R. M. *J. Am. Chem. Soc.* **2005**, *127*, 4930.
(22) Petrii, O. *J. Solid State Electrochem.* **2008**, *12*, 609.
(23) Markovic, N. M.; Ross, P. N. *CATTECH* **2000**, *4*, 110.
(24) Tian, N.; Zhou, Z.-Y.; Sun, S.-G. *J. Phys. Chem. C* **2008**, *112*, 19801.
(25) Bönnemann, H.; Khelashvili, G. *Appl. Organomet. Chem.* **2010**, *24*, 257.
(26) Gu, Y.; Wu, G.; Hu, X. F.; Chen, D. A.; Hansen, T.; zur Loye, H.-C.; Ploehn, H. J. *J. Power Sources* **2010**, *195*, 425.
(27) Stamenkovic, V. R.; Fowler, B.; Min, B. S.; Wang, G.; Ross, P. N.; Lucas, C. A.; Markovic, N. M. *Science* **2007**, *315*, 493.
(28) Alayoglu, S.; Nilekar, A. U.; Mavrikakis, M.; Eichhorn, B. *Nat. Mater.* **2008**, *7*, 333.
(29) Alayoglu, S.; Eichhorn, B. *J. Am. Chem. Soc.* **2008**, *130*, 17479.
(30) Peng, Z.; Yang, H. *Nano Today* **2009**, *4*, 143.
(31) Pellechia, P. J.; Gao, J.; Gu, Y.; Ploehn, H. J.; Murphy, C. J. *Inorg. Chem.* **2004**, *43*, 1421.
(32) Lafaye, G.; Williams, C. T.; Amiridis, M. D. *Catal. Lett.* **2004**, *96*, 43.
(33) Gu, Y.; Xie, H.; Gao, J.; Liu, D.; Williams, C. T.; Murphy, C. J.; Ploehn, H. J. *Langmuir* **2005**, *21*, 3122.
(34) de la Fuente, J. L. G.; Rojas, S.; Martínez-Huerta, M. V.; Terreros, P.; Peña, M. A.; Fierro, J. L. G. *Carbon* **2006**, *44*, 1919.
(35) Antolini, E. *Mater. Chem. Phys.* **2003**, *78*, 563.
(36) Yajima, T.; Uchida, H.; Watanabe, M. *J. Phys. Chem. B* **2004**, *108*, 2654.
(37) Chin, S. Y.; Williams, C. T.; Amiridis, M. D. *J. Phys. Chem. B* **2006**, *110*, 871.
(38) Park, S.; Wasileski, S. A.; Weaver, M. J. *J. Phys. Chem. B* **2001**, *105*, 9719.

(39) Arenz, M.; Mayrhofer, K. J. J.; Stamenkovic, V. R.; Blizanac, B. B.; Tomoyuki, T.; Ross, P. N.; Markovic, N. M. *J. Am. Chem. Soc.* **2005**, *127*, 6819.
(40) Babu, P. K.; Kim, H. S.; Kuk, S. T.; Chung, J. H.; Oldfield, E.; Wieckowski, A.; Smotking, E. S. *J. Phys. Chem. B* **2005**, *109*, 17192.
(41) Zhao, M.; Crooks, R. M. *Angew. Chem., Int. Ed.* **1999**, *38*, 364.
(42) Zhao, M.; Crooks, R. M. *Adv. Mater.* **1999**, *11*, 217.
(43) Buffat, P.-A.; Flüeli, M.; Spycher, R.; Stadelmann, P.; Borel, J.-P. *Faraday Discuss.* **1992**, *92*, 173.
(44) Pan, C.; Dassenoy, F.; Casanove, M.-J.; Philippot, K.; Amiens, C.; Lecante, P.; Mosset, A.; Chaudret, B. *J. Phys. Chem. B* **1999**, *103*, 10098.
(45) Aiken, J. D., III; Finke, R. G. *J. Mol. Catal. A: Chem.* **1999**, *145*, 1.
(46) Conway, B. E.; Tilak, B. V. *Electrochim. Acta* **2002**, *47*, 3571.
(47) Maillard, F.; Eikerling, M.; Cherstiouk, O. V.; Schreier, S.; Savianova, E.; Stimming, U. *Faraday Discuss.* **2004**, *125*, 357.
(48) Maillard, F.; Lu, G.-Q.; Wieckowski, A.; Stimming, U. *J. Phys. Chem. B* **2005**, *109*, 16230.
(49) Jusys, Z.; Kaiser, J.; Behm, R. J. *Electrochim. Acta* **2002**, *47*, 3693.
(50) Brankovic, S. R.; Marinkovic, N. S.; Wang, J. X.; Adzic, R. R. *J. Electroanal. Chem.* **2002**, *532*, 57.
(51) Kuk, S. T.; Wieckowski, A. *J. Power Sources* **2005**, *141*, 1.
(52) Gasteiger, H. A.; Kocha, S. S.; Sompalli, B.; Wagner, F. T. *Appl. Catal., B* **2005**, *56*, 9.
(53) Lee, G.; Shim, J. H.; Kang, H.; Nam, K. M.; Song, H.; Park, J. T. *Chem. Commun.* **2009**, 5036.

JP106728S